Biochimica et Biophysica Acta, 690 (1982) 187–198
Elsevier Biomedical Press

BBA 71303

X-RAY DIFFRACTION ANALYSIS OF WET ISOLATED BOVINE ROD OUTER SEGMENT DISKS

A DEHYDRATION STUDY *

SOL M. GRUNER **, DANIEL T. BARRY *** and GEO T. REYNOLDS

Joseph Henry Laboratory, Department of Physics, Princeton University, P.O. Box 708, Princeton, NJ 08544 (U.S.A.)

(Received March 5th, 1982)

Key words: X-ray diffraction pattern; Electron density profile; Rhodopsin; Rod outer segment; Dehydration

Sequences of X-ray diffraction patterns were obtained from dehydrating, artificially oriented multilayers of isolated, bovine rod outer segment disks. A direct-phase analysis was applied to highly hydrated specimens to determine sequences of low resolution (approx. 30 Å) electron density profiles of the disks as dehydration proceeded. The profiles were found to evolve smoothly as the multilayer lattice simultaneously shrank and became increasingly ordered. The bilayer profiles were largely invariant under dehydration and the evolution of the diffraction consistent with simple decreases in fluid spacings. The specimens were observed to phase separate into characteristic primary and a secondary lattices when the multi-layer became too dehydrated. The small unit cell size of the secondary lattice was suggestive of a lipid phase. Large changes in the diffraction patterns from phase separated specimens were observed upon bleaching of the specimen. The changes were consistent with a reversible disordering of the primary lattice.

Introduction

Despite numerous investigations, the transmembrane organization of the vertebrate retinal rod outer segment disk is still in dispute. Attempts to determine the organization by analysis of the X-ray diffraction from whole rod outer segments have been hampered largely because of two reasons: first, stacking disorders of the rod outer segment disks limit the data to a resolution of $(2 \sin\theta)/\lambda \simeq 1/(25\ \text{Å})$ (i.e., 11th order of a roughly 300 Å repeat). Thus, high resolution detail is absent in the electron density profiles [3]. Second, the interpretation of the membrane profile is ambiguous. The interpretation would be aided if one could chemically label the disks and observe the effects upon the profile. This cannot easily be done because the disks are sealed in the rod outer segments.

An alternative approach is to rupture the rod outer segments, extract the disks, and artificially stack them into a multilayer. This approach has been used by Blasie and co-workers [4–8] to collect lamellar diffraction from centrifugally oriented and partially dehydrated isolated disks. Diffraction was observed to a resolution of 8 Å. It was realized, however, that the diffraction was due to a complex phase separated specimen which included more than one kind of lattice (Blasie, J.K.; Saibil, H.; Santillan, G.; personal communi-

* An abstract of this study was presented at the annual meeting of the Biophysical Society, 1980 [1]. Much of the material presented in this article may also be found in the Ph.D. thesis of D.T. Barry [2].

** To whom correspondence should be addressed.

*** Department of Physical Medicine and Rehabilitation, Box 33, University of Michigan Hospital, 1405 E. Ann Street, Ann Arbor, MI 48105, U.S.A.

cations). Consequently, the profiles could not be unambiguously determined. Moreover, it was apparent that the phase separation occurred at some point in the dehydration process.

In this article we describe the behavior of isolated disk specimens as a function of hydration. The importance of such a study is 2-fold: First, if isolated disk profiles can be reliably determined as long as the multilayers are sufficiently hydrated, then it may be possible to examine the effects of chemical modification of the disks. An important example of this would be the effect of the removal or addition of the peripherally bound, non-rhodopsin disk proteins that are believed to play a role in visual transduction [9]. A second reason for studying the disks as they dehydrate is to attempt to understand what the phase separation phenomenon implies about the structure of the disk.

Material and Methods

Specimen preparation

Several disk isolation procedures were examined by electron microscopy to determine which one least disrupted the disks. The results of this study and the detailed isolation procedure (Metriz.-Ficoll-no(ConA) may be found in Ref. 10 by Barry et al. In summary, rod outer segments were isolated from freshly excised bovine eyes by means of a metrizamide gradient. The rod outer segments were hypotonically ruptured and the disks collected by a Ficoll flotation. These were then washed with Ringers solution several times and suspended in Ringers. No additional steps were taken to remove Ficoll which may have remained. Throughout, care was taken to keep the disks in a cold (4°C) and deoxygenated environment. All work was done in darkness or under dim red lights. Typical yields were 0.5 mg of rhodopsin per retina.

The purity of the disk material was assayed spectrophotometrically and via sodium dodecyl sulfate polyacrylamide gel electrophoresis. The absorbance ratio, at 280 and 498 nm, of detergent solubilized disks is a measure of the relative fraction of unbleached rhodopsin [11]. Typical values were 2.4. Gel electrophoresis indicated the disk protein to be predominantly rhodopsin with a small complement of accessory disk proteins.

The X-ray specimens were formed by pelleting an aliquot of the suspension (containing approx. 0.25 mg of rhodopsin) at $80000 \times g$ for 2 h onto an aluminum foil or Saran plastic substrate in a lucite sedimentation cell [4,5]. The sedimention cell yielded a thin specimen pellet (4 mm in diameter) adhering to the substrate. The substrate was then wrapped around a section of an aluminum cylinder of 4 cm radius. The specimen was either used immediately or stored overnight, on ice, in a bottle which had been purged with water-saturated argon. The specimen assembly was clipped into the X-ray specimen chamber with minimal exposure (< 1 min) to air. The cold (4–5°C) chamber was immediately purged with most helium. The relative humidity of the helium was varied over the range of 95 to 85% by slow circulation of the gas through saturated salts or through a humidity generator [12]. The specimen was bleached, in situ, by a tungsten lamp via a lucite light guide.

The absorbance ratio of 250 nm to 280 nm was used to assay lipid oxidation [13]. By using the oxidation control procedure of Stone et al. [14] the ratio of the disk suspension could be kept consistently below 0.5. To determine if the pelleted specimens were being oxidized, representative X-ray specimens were spun onto quartz slides. The 250/280 ratio of these specimens was stable unless the pellets were deliberately exposed to air.

Instrumentation

Nickel filtered CuKα ($\lambda = 1.54$ Å) X-rays were generated on a Jarrel-Ash microfocus generator run at an anode loading of 40 kV and 5–7 mA. X-rays were collimated and focused using guard slits and single mirror Franks optics. The X-ray beam was spectrum analyzed utilizing calibrated photomultiplier-scintillator combinations. A typical flux was 10^7 X-rays/s, which was 93% CuKα, into a 0.2×3 mm tall beam at the specimen. The beam was set to graze the specimen tangentially, i.e., parallel to the average membrane plane. A vacuum path was placed between the specimen chamber and the detector. This apparatus is described in detail in Ref. 8.

Isolated disk multilayers dehydrate very easily. It was necessary to record successive data sets, each several minutes in duration, to track the behavior of the specimen as it slowly lost water to

the moist helium gas. This was made possible by the development of a quantum-limited image-intensified-TV X-ray area detector, described in detail elsewhere [8,15–18]. In brief: the X-ray image was converted to a light image by a thin phosphor screen and the light image was intensified. The image intensifier had sufficiently high gain that each absorbed X-ray was clearly visible. The optical image was recorded by a special TV camera tube run in a slow-scan, integrating mode. The output of the camera was digitized and stored on a computer disk. This output is a matrix of 240×240 numbers corresponding to the X-ray itensity of a 240×240 grid on the scintillating screen.

Data reduction

The detailed data correction and reduction procedures may be found in Ref. 2. The data were first corrected for the known detector uniformity and geometric distortions [18]. A polarization correction was then applied. The diffuse ring at $1/(4.6$ Å), presumed to be due to the fluid lipid hydrocarbons in the membranes, was monitored over a range of angles to determine the absorption correction [6]. It was found that, over the small range of angles used in this study, no absorption correction was needed. The data were reduced to a one-dimensional function of X-ray intensity vs. reciprocal radius by integrating over arcs within ± 5 degrees of the lamellar axis. (The lamellar $\equiv$ meridional axis is defined to be parallel to the multilayer stacking axis.) Since an integration over angle was used, a Lorentz correction proportional to the reciprocal coordinate, s, was applied. The effects of the point spread of the detector, and, to a great extent, the finite beam height were removed during the data analysis. This was done by deconvoluting an integration of the attenuated incident beam during the calculation of the lattice disorder (see data analysis procedure, below). This had little effect on the analysis because the diffracted peaks were very broad (due to disorder) and because the coherent diffraction immediately adjacent to the beam stop was weak. The background scatter was determined from blank substrates and by noting the X-ray intensity from specimens at 90° to the lamellar axis. The latter intensity could not be used directly as a background subtraction because of arcing of the high mosaic spread lamellar reflections. The underlying background was always well fit by an exponential in all but the very low angle region, where the background was steeper. A first order reflection could be distinguished in the very low angle region. Although the presence of this order was very important in assigning the unit cell dimension, its intensity was extremely weak relative to the other lamellar reflections. Inclusion of a reflection of this intensity in the analysis did not affect the resultant profiles to within the error bars. Consequently, the very low angle scatter was usually truncated at the first minimum after exponential subtraction, even though the truncated data included the first order. The truncation points are indicated by arrows in Fig. 1. The specimens had to be advanced into the X-ray beam as they dehydrated because the dehydration reduced the specimen thickness and caused the specimen surface to move out of the beam.

Error bars in the diffraction pattern were calculated according to the procedures described in Refs. 2 and 8. The error bars in the electron-density profile reflect the statistical quality of the data, not the systematics of the analysis. Thus, errors due to the selection of the locations of the zeros, truncation, and the phasing are not represented (see Application of the data analysis, below).

In what follows, the reciprocal coordinate $\equiv s = (2 \sin \theta)/\lambda$, where 2θ is the diffraction angle and λ is the X-ray wavelength.

Data analysis procedure

The nomenclature of the results section can be best understood by considering the data analysis procedures in detail: In an ideal X-ray experiment one records the X-ray intensity, $I(s)$, a quantity proportional to $|F(s)|^2$, where

$$F(s) \equiv f[\rho(x)] \tag{1}$$

Here, $\rho(x)$ is the specimen electron density distribution projected onto the sedimentation axis, s, and $f[\,]$ denotes the Fourier transformation operation. Since only the modulus of $F(s)$ is determined, Eqn. 1 cannot, in general, be uniquely inverted to determine $\rho(x)$. If $\rho(x)$ is centro-symmetric then its Fourier decomposition must be

purely a sum of cosinusoidal terms. In this case, $F(s)$ is real and differs from $|F(s)|$ only by values of sign. Hosemann and Bagchi [19] pointed out that a specimen consisting of a small number of symmetric unit cells yields diffraction which (up to an overall sign and additive constant) is unique to $\rho(x)$. They also pointed out the existence of numerical procedures for recovering $\rho_0(x)$, the 'unit cell' electron density distribution, from $F(s)$ (see Worthington et al. [20] for a review of these procedures). Thus, if suitable symmetry of the specimen may be assumed, $\rho_0(x)$ can be recovered directly from $F(s)$; such procedures have been termed direct phase procedures. The difficulty with these methods is the practical constraint of the number of unit cells in the latice: if the number is too large the line widths needed for the analysis become difficult to measure; if too small, the overall diffraction becomes weak.

An arbitrary membrane with an asymmetric bilayer can be made into a centro-symmetric lattice by stacking flattened vesicles of the membrane. In this case, the unit cell encompasses two bilayers with a center of symmetry between them. Ideally, the rod outer segment itself is such a lattice. However, in both the cases of the rod outer segment and artificial vesicle multilayers, variation of the widths of the fluid spaces between the membranes imparts disorder to the multilayer lattice. Analysis of the diffraction from a disordered, symmetric membrane lattice, namely the intact rod outer segment, was treated by Schwartz et al. [3]. A similar procedure was later applied by Nelander and Blaurock [21] to diffraction from myelin.

The analytical procedure used in the present study closely follows Ref. 3. This procedure approximates the distributions of fluid spacing widths by Gaussianly distributed distances. Two such distributions are assumed to characterize the sample: The first is the variation in the placement of the unit cells, termed lattice disorder. This leads to coherently diffracted intensity, $I_c(s)$, given by [22]

$$I_c(s) = |F_0(s)|^2 \cdot Z(s) * |\Sigma(s)|^2 \tag{2}$$

where

$$Z(s) = \frac{1-\beta^2}{1+\beta^2-2\beta\cos(2\pi ds)} \tag{3}$$

$\beta = \exp(-2\pi^2 s^2 \sigma^2)$
d = average unit cell repeat distance
σ = standard deviation in d.
and $*$ represents the convolution operation.

Here $F_0(s)$ is the transform of the projected unit cell electron density distribution, $\rho_0(x)$, $Z(s)$ is the sampling function, and $\Sigma(s)$ is the form factor [22].

The second distribution characterizes the variation within the unit cell. This variation, termed substitution disorder, leads to incoherent X-ray scatter, $I_i(s)$. The total scatter, $I(s)$ is the sum

$$I(s) = I_c(s) + I_i(s) \tag{4}$$

It is assumed that the lattice and substitution disorders are independent of one another. The Schwartz et al. [3] procedure for separating the coherent and incoherent intensities was used for this paper.

Application of the data analysis

The disorders present in the highly hydrated specimens were considerably greater than those encountered in rod outer segment. Consequently, the application of the Schwartz et al. [3] procedure to highly disordered lattices was examined. Hypothetical electron density profiles were fit in lattices with various amounts of lattice and substitution disorders. These were Fourier transformed to simulate the diffraction expected from such a lattice. Noise was added to simulate the X-ray statistics. Let $\bar{a}$ represent the average bilayer midplane to bilayer midplane distance across the intra-diskal (i.e., lumen) space. Assume this distance distributes as a normalized Gaussian probability of e^{-1} width $= \alpha$. Then, as long as the substitution disorder remained small ($\alpha/\bar{a} < 0.05$), profiles were systematically recovered. However, once the substitution disorder became large ($\alpha/\bar{a} > 0.15$), it was necessary to include additional information (e.g., knowledge of a bilayer-type structure, or phase information) to reliably recover the initial profile.

The more highly hydrated specimens (see below) had significant substitution disorder ($\alpha/\bar{a} =$ 0.1 to 0.2). It was necessary to use information in addition to the individual experimental intensities. It was observed that $|F(s)|$ varied smoothly as the

specimen dried. Consequently, it was assumed that the signs of the non-zero parts of $F(s)$ (i.e., the regions of $|F(s)|$ between zeros (see Fig. 2) did not change as the specimen dried. Thus, the phase choices for the X-ray intensities from the drier history of the specimen could be extrapolated to the intensities from when the specimen was wetter. As shown below, this is consistent with the assumption that the effect of drying is to decrease the width of the fluid spaces. This was the assumption used by Corless [23] and Blaurock and Wilkens [24], in shrinking and swelling experiments of rod outer segment. A bilayer membrane structure was not assumed. The bilayer structure was the one which was consistently generated by the analysis. Furthermore, no assumption was made relating structures from one experiment to the next. Again, the similarities came directly from the data.

For the broad peaks considered in this study, the form factor in Eqn. 2 can be approximated as a δ-function. The coherent intensity is then given by $I_c(s) = |F(s)|^2 \cdot Z(s)$. Since $Z(s) > 0$ for all s,

$$|F_0(s)|^2 = \frac{I_c(s)}{Z(s)} \tag{5}$$

The inverse Fourier transform of $I_c(s)$ is called $Q(x)$, the generalized Patterson function; it is the autocorrelation function of the multilayer. $Q(x)$ is pseudoperiodic in d, the average unit cell spacing, and can therefore be used to aid the determination of d. The value of d determined was used with various values of σ, the standard deviation of the unit cell spacing, to generate trial sampling functions, $Z(s)$, using Eqn. 3. The correct $Z(s)$ was identified by inverse Fourier transforming the resultant $|F_0(s)|^2$, using Eqn 5, to obtain the unit cell autocorrelation function $Q_0(x)$. A correct $Q_0(x)$ must equal zero for $|x| > d$. The $Z(s)$ which minimized deviations of Q_0 outside d was used.

In practice, the $|F_0(s)|^2$ obtained often had large, sharp peaks near the origin where $Z(s)$ became close to zero. These peaks were truncated before proceeding with the analysis. Sometimes a $Z(s)$ which fit a low angle peak was too narrow or too broad for a higher angle peak, particularly when the data contained secondary lattice reflections. This was used as a means of detecting phase separation.

Once $|F_0(s)|^2$ has been obtained, one applies the straightforward technique of trying every possible phase combination and comparing the autocorrelation function which results from each choice with the experimentally obtained autocorrelation function, $Q_0(x)$. The phase choices which are closest to the actual phase combination are revealed by a good fit between the calculated and experimental generalized Patterson functions [3].

Specimen constraints

A specimen must meet a number of constraints in order that the diffraction pattern it yields be meaningful if analyzed by the direct phasing procedures described above. These constraints are that the specimen

(1) must have a unique and unambiguous lattice spacing,
(2) must be uniformly of a single chemical phase,
(3) must be stable over periods of time long compared with the time required to collect the data,
(4) must yield statistically adequate coherent diffraction to the calculated resolution,
(5) must be a uniform population of single-walled, univerted vesicles.

Specimens were determined to have met the constraints on the basis of the X-ray data recorded as the specimens were dehydrated and on the basis of a freeze-fracture electron miscroscope study. The first two constraints were violated if the specimens became too dehydrated: X-ray reflections appeared which could not be indexed on the primary Bragg lattice and whose width was too sharp to be consistent with the primary lattice sampling function, $Z(s)$. This indicated specimen phase separation. A well-behaved $Z(s)$ exhibits reflections which are sharp at the origin and monotonically broaden with higher order number (see, for example, Fig. 1). One can never be certain that some small part of the specimen has not phase separated; rather, one seeks specimens in which the phase separation is negligible. Diffraction from even moderately phase-separated specimens was easily recognized.

Stability of the specimen was verified by looking for differences in sequential data sets. In these experiments, the specimen was dehydrated continuously; consequently, the diffraction evolved

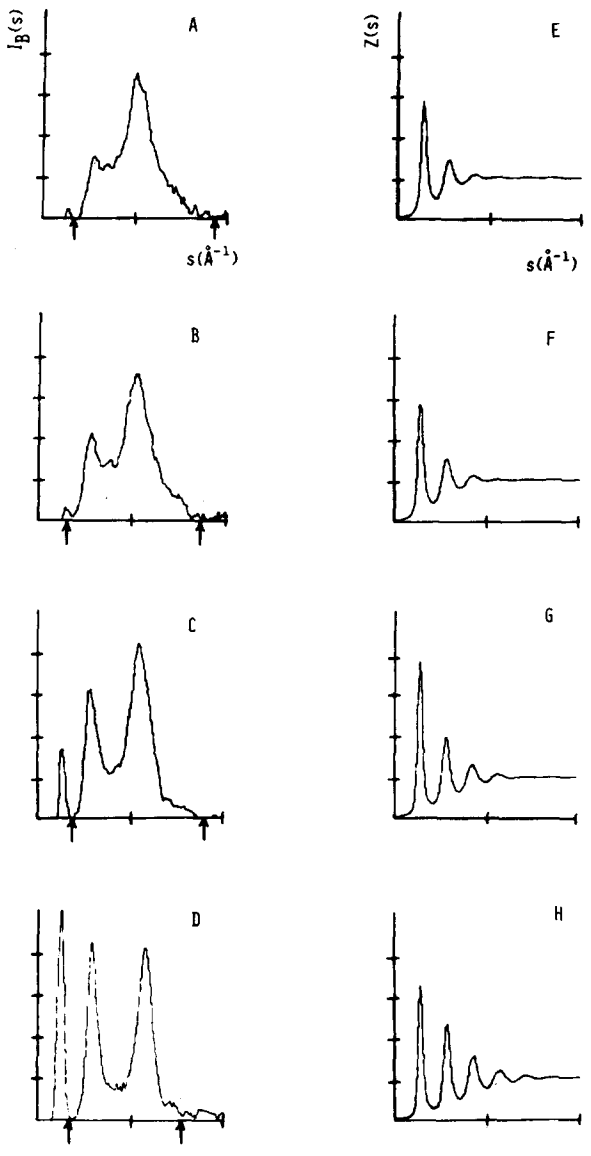

Fig. 1. Conventions for all figures except Fig. 5: Figures which have reciprocal space distances as an abscissa are labelled by $s(Å^{-1})$ at the top of the column. Abscissa tic marks are every 0.02 $Å^{-1}$. Figures which have real space distances as an abscissa are labelled by $x(Å)$ at the top of the column. These have abscissa tic marks every 20 Å. All ordinates are in arbitrary units. Error bars are occasionally shown. An analysis of a high water content specimen at four different times, corresponding to four states of hydration, is shown. A given row across Figs. 1, 2, and 3 represents the analysis of one hydration state of the same specimen. The most highly hydrated state is represented by the top row; the least by the bottom row. Parameters of the analysis are in Table I. The background subtracted intensities, $I_B(s)$ (A–D), and the sampling functions, $Z(s)$ (E–H), are shown in Fig. 1. The data outside of the arrows were truncated (see text).

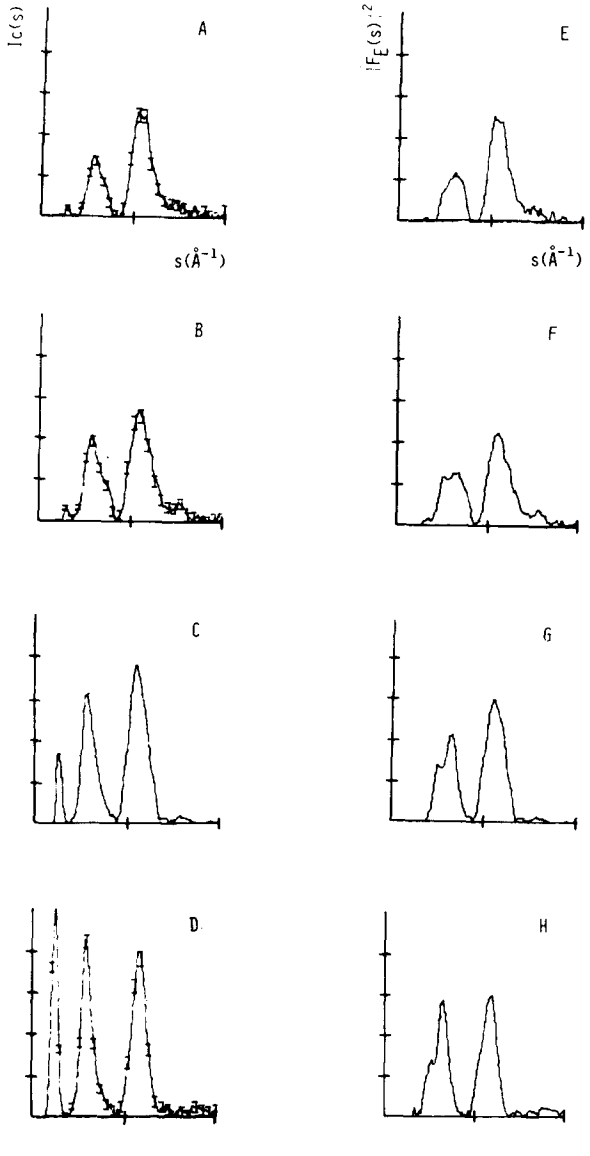

Fig. 2. A continuation of the analysis from Fig. 1 (see Fig. 1 caption). The coherent intensity $I_c(s)$ (A–D), and the experimental squared structure factors, $|F_E(s)|^2 = I_c(s)/Z(s)$ (E–H), are shown.

Fig. 3. (p. 193). A continuation of the analysis from Figs. 1 and 2 (see prior figure captions). The unit cell electron density profiles $\rho(x)$ (A–D), and the computed squared structure factors, $|F(s)|^2$ (E–H) are shown.

TABLE I

LATTICE PARAMETERS OF THE DISC MULTILAYER

d = lattice constant (unit cell spacing); σ = standard deviation in d (lattice disorder); $\bar{a}$ = average spacing of membranes within a unit cell; $\alpha = 1/e$ width of Gaussian distribution about $\bar{a}$ (substitution disorder). Time = 0 is when recording of the diffraction from the specimen began.

Fig. 2	Time	Lattice (Å)		Membrane spacing (Å)		Structure factor	
		d = Repeat	σ = Disorder	$\bar{a}$ = Distance	α-Disorder	Zeros ($Å^{-1}$)	Phases
A	0 h	180	24	90	17	0.017, 0.0275	+ − +
B	1 h 13 min	175	22	87.5	16	0.017, 0.028	+ − +
C	3 h 6 min	178	17.5	87	12	0.018, 0.029	+ − +
D	5 h 11 min	176	14.5	86	8.5	0.018, 0.028	+ − +

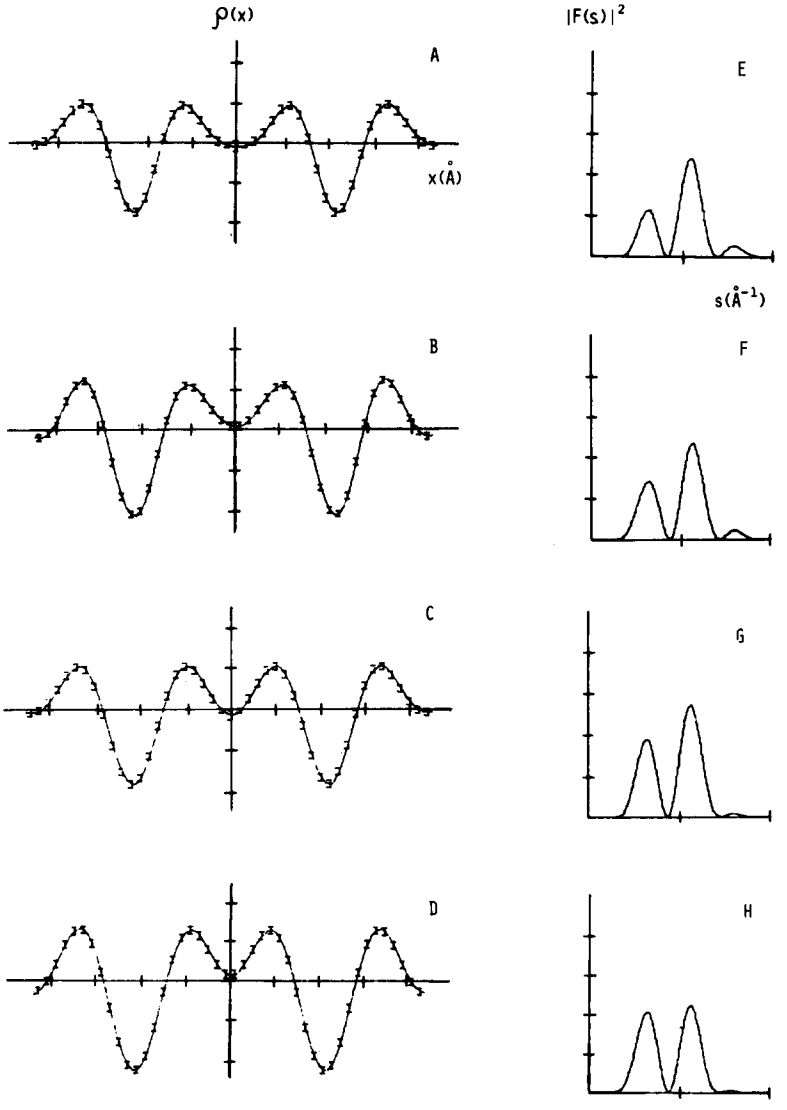

continuously over the course of several hours. The area detector allowed data sets to be accumulated in several 'exposures', each a few hundred seconds long. In general, exposures were summed until the difference between the first and last exposures in a data set were comparable to the statistical uncertainty in those exposures. The fourth constraint determined the resolution of the profiles. Coherent diffraction was observed beyond the approx. 30 Å resolution of this study. However, the statistical adequacy of these data was deemed too poor for a direct phasing; consequently, the data were truncated at a minimum at $s \simeq 0.033$ Å.

The final constraint is violated if an appreciable fraction of the disks are inverted or multi-walled. If the membrane is asymmetric, then inversion or vesicles within vesicles without inversion represents a variation in the unit cell structure. The procedure that has been used to prepare the X-ray specimens was selected after a freeze-fracture electron microscope study of several methods of disk isolation [10]. The study indicated that no more than 1% of the disks were inverted. Roughly 5% of the disk vesicles contained other vesicles. However, since the inner vesicles were generally small, the fraction of the specimen which was disturbed in this way was smaller than 5%.

Results

High water content specimens

Specimens which had just been removed from the sedimentation cell were mostly water. These were transferred to the X-ray apparatus and their dehydration was tracked with the X-ray detector. Figs. 1 and 2 and Table I illustrate the progressive changes in a high water content specimen as it dehydrated. Figs. 1A–1D illustrate the evolution of the background subtracted data for a representative experiment. The sampling function is shown in Figs. 1E–1H, the coherent experimental intensity in Figs. 2A–2D, and the experimental structure factor moduli in Figs. 2E–2H. The proposed electron density profiles are shown in Fig. 3. It is observed that as the specimen dries, the X-ray reflections become sharper and more intense (Figs. 1A–1D). This is manifest in an increasingly modulated sampling function (Figs. 1E–1H). The initial effect upon the sampling function is a slight decrease in the lattice constant represented by an expansion in the spacings between the sampling function peaks (Figs. 1E and 1F and rows A and B in Table I). Thereafter, the lattice constant is almost constant but the sampling function becomes increasingly modulated as the disorder within the lattice decreases (Figs. 1G and 1H and Table I). The statistical quality of the data was inadequate for a profile reconstruction at a resolution higher than approx. $(30\ \text{Å})^{-1}$: consequently, the data were truncated at this value (Fig. 1). At this resolution the profiles (Fig. 3) appear to be nearly symmetrical bilayers.

The changes in the diffraction are consistent with a decrease in the width of the fluid spaces between the membranes: In Fig. 4C we have taken the profile of Fig. 3C and drawn in progressively wider fluid spaces (Figs. 4A and 4B). These were Fourier transformed to obtain the structure factor moduli $|F(S)|^2$, shown in Figs. 4D–4F. The primary effect upon the moduli is to decrease the height of the peak at approx. $0.03\ \text{Å}^{-1}$ and increase that at approx. $0.01\ \text{Å}^{-1}$. Simultaneously, all the zeros shift away from the origin. Note how the trends in these moduli agree with those actually found for the variously hydrated states of the specimen (Figs. 2E–2G).

Low water content specimens

As the specimen dehydrates further, the lamellar reflections become progressively sharper and more intense. This process continues until the unit cell shrinks below roughly 150 Å, at which point the diffraction patterns change dramatically. The first order, which has been weakly present throughout, becomes considerably more intense. This is soon accompanied by the appearance of other orders which index with odd integers (data not shown). This is followed by the appearance of additional orders which cannot be indexed on the primary lattice constants. This is clearly shown in Fig. 5. Here, the primary lattice indexes with a 143 Å repeat. An additional set of reflections which are characterized by a 58 Å repeat may also be seen.

The phase separated data cannot easily be used to generate electron-density profiles but the sharp lines and high detail allow examination or the effects of bleaching of the disks. Both Santillan [6]

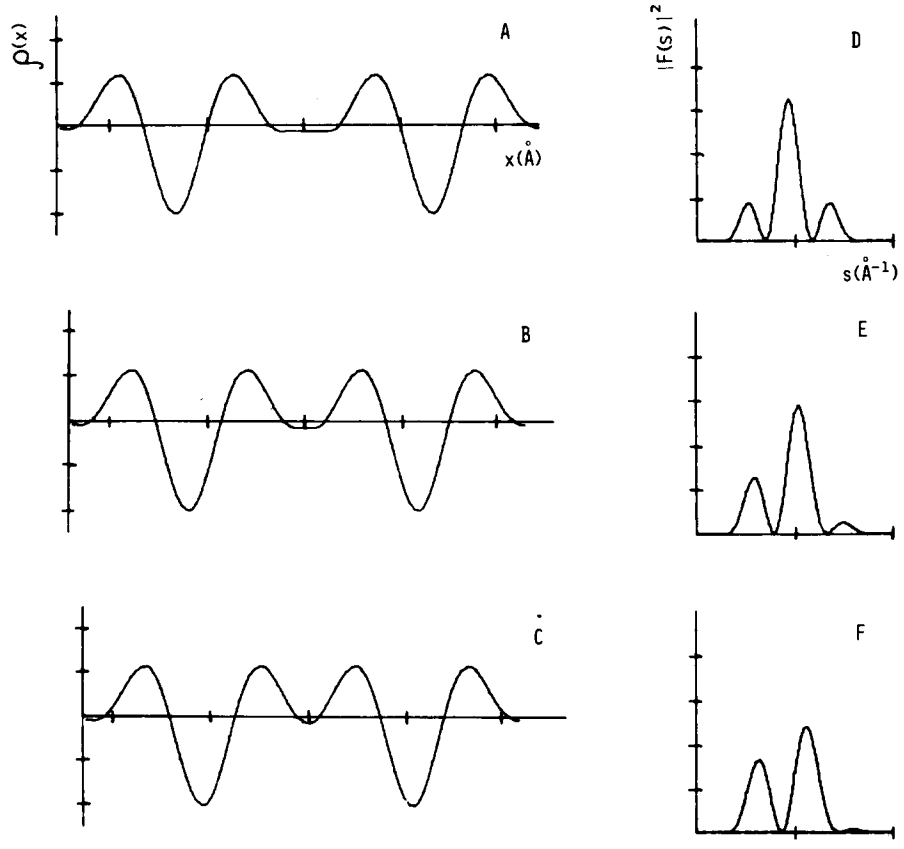

Fig. 4. A computer model showing how the qualitative evolution of $|F(s)|^2$ can be largely accounted for by a variable fluid space (see text). The most hydrated figure is at the top so as to be directly comparable to Fig. 3.

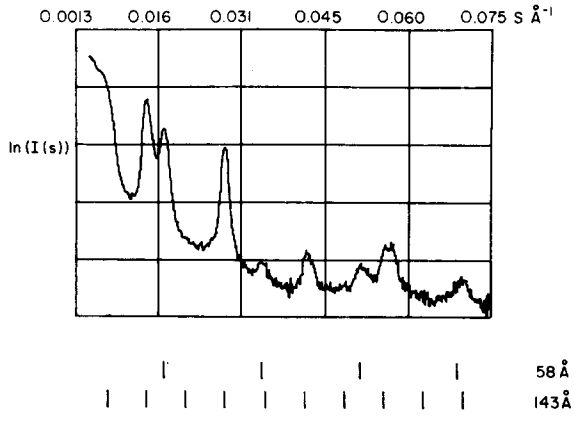

Fig. 5. Diffraction, on a log scale, from a phase-separated specimen. The two sets of tic marks indicate the expected Bragg peak positions from a 58 and a 143 Å repeat along the lamellar axis. These are raw diffractometer data acquired at the Stanford Synchrotron Radiation Laboratory at Stanford, CA. The integration time is 20 s/pt.

and Gruner [8] reported changes in the diffraction upon bleaching. The speed advantage of the image-intensified detector allowed the time-course of the changes to be followed: Fig. 6 shows a series of diffraction patterns before and after bleaching. The effect of light is to shorten and widen the diffraction lines. This is interpreted as resulting from an increase in the lattice disorder within the specimen. Interestingly, the secondary lattice does not seem to be affected as much as the primary lattice. Furthermore, some of the changes with bleaching are transitory. Fig. 6I shows that the sharpness and height of the reflections have largely returned within approx. 2 h after bleaching was started. It would be difficult to observe such transitory effects with film as a detector. We note that both Chabre [25] and Schwartz et al. [3] (analyzing Chabre's data) reported a disordering of the lattice

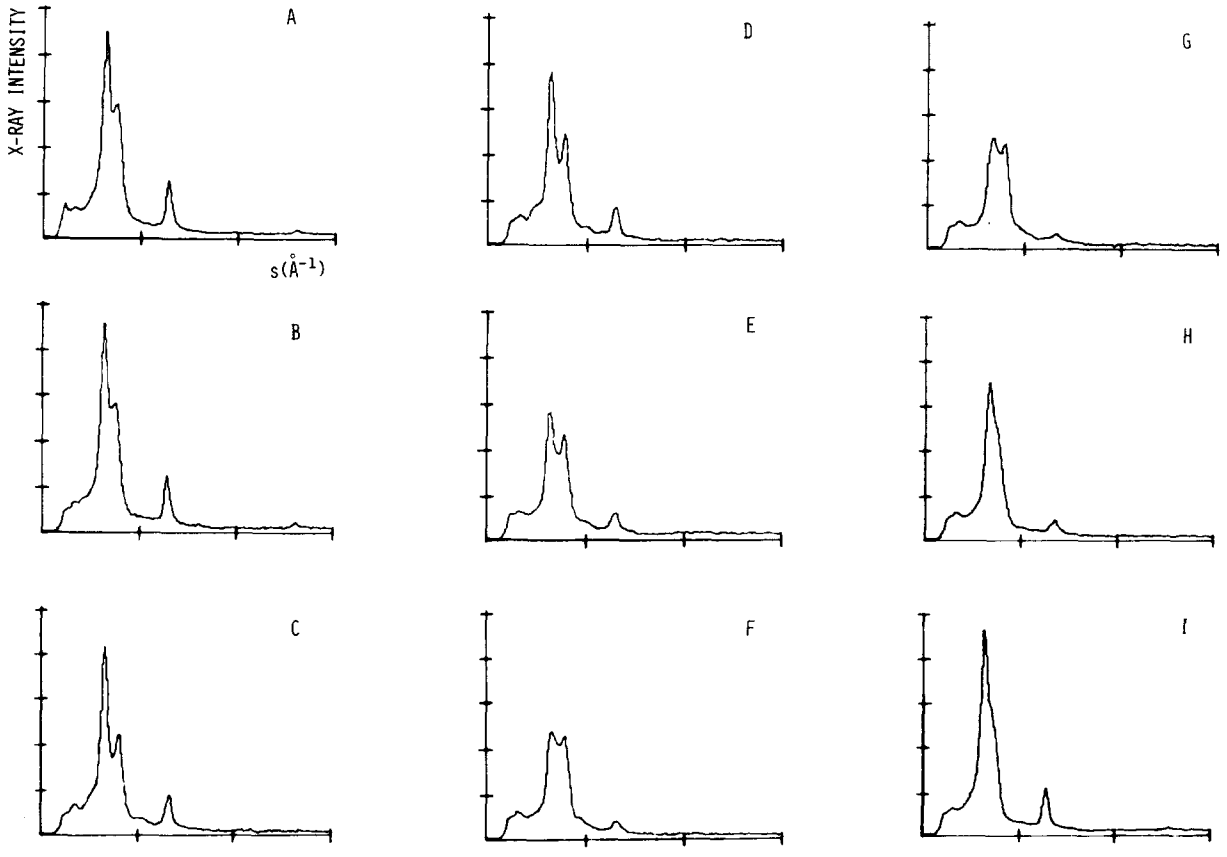

Fig. 6. Changes in the diffraction upon bleaching a low water content specimen are shown. The data have only been correected for the detector nonuniformity. (A) 1440 s exposure taken 2 h 21 min before bleaching. The intensity has been normalized by the exposure ratio = 120/1440. (B) 120 s exposure taken immediately before bleaching. (C) 120 s exposure begun immediately after bleaching started. (D) 120 s exposure begun 2 min after bleaching started. (E) 120 s exposure begun 7 min after bleaching started. (F) 120 s exposure begun 18 min after bleaching started. (G) 240 s exposure begun 21 min after bleaching started. The intensity has been normalized by the exposure time ratio = 120/140. (H) 560 s exposure begun 30 min after bleaching started. The intensity has been normalized by the exposure time ratio = 120/560. (I) 1120 s exposure begun 1 h 54 min after bleaching started. The intensity has been normalized by the exposure time ratio = 120/1120.

upon the bleaching of intact rod outer segment. The reason the lattice disorders upon bleaching is not understood.

Discussion

The continuous dehydration experiments of high water content specimens present a consistent picture of the dehydration dynamics. The reduction in unit cell dimension, bilayer spacing and specimen disorder are all indicative of an overall contraction and equilibration of the specimen in which the forces acting on the lattice compress it and restrict its freedom toward disorder. The low resolution bilayer profiles appear largely symmetric and invariant in this process. Modeling studies suggest that the dominant features of the data are consistent with a variable fluid space between the membranes.

A dramatic reorganization of the specimen begins to occur when the unit cell repeat approaches 150 Å. The appearance of odd orders indicates that the unit cell profile contains two asymmetric halves, i.e. wheras the more hydrated unit cell was nearly symmetric about each of the two bilayer midplanes, the drier unit cell is only nearly symmetric about one central midplane. Such an asymmetrization would occur if the intra- vs. inter-disk

fluid spaces were of different average thicknesses, if the electron density of the bilayers were to redistribute asymmetrically along a normal to the membrane plane, or if the membrane had prominent features on one surface which interdigitated with the features on the adjacent membrane surface. We currently have insufficient evidence to distinguish among the possibilities. The data do strongly suggest, however, that one surface of the bilayer is very different from the other surface. This difference is manifest by whatever forces lead to an asymmetrization of the unit cell when the opposing bilayers are brought into close proximity.

Further reduction in the unit cell repeat is accompanied by a phase separation of the specimen. This is indicated by two sets of generally incommensurate diffracted orders. At certain hydrations the diffraction from the two phases can be nearly commensurate. This led Santillan [6] and Gruner [8] to incorrectly ascribe the diffraction to a single large unit cell. It was soon realized, however, that all the reflections could not be indexed on a single lattice as the humidity was varied.

The data shown in Fig. 5 can be most simply explained by assuming that the specimen is characterized by a large and a small lamellar lattice. The large lattice evolves continuously from the hydrated, primary lattice. Moreover, even highly phase separated specimens continue to exhibit meridional 5 Å and equatorial 10 Å reflections [6,8]. These reflections are ascribed to the secondary structure of oriented membrane protein [26]; they do not appear in the lamellar diffraction from extracted rod outer segment lipids [6]. This suggests that the membrane protein in the phase separated samples has not completely denatured and is still oriented in a lamellar phase. We suggest that the larger phase separated lattice is a protein containing lamellar phase.

The smaller repeat of the secondary lattice is suggestive of a lipid phase. Protein-lipid phase separations have been observed in a number of membranes [27]. The simplest explanation for the data of Fig. 5 is that the specimen consists of two co-existing lamellar phases. However, we have obtained unequivocal evidence that the secondary phase observed in vacuum dehydrated disk specimens [28,29] is a hexagonal lipid phase oriented such that a set of hexagonal crystal planes are parallel to the membrane lamellae (Gruner, Rothschild and Clark [30]). In this case, the only indication that one is not dealing with a lamellar lipid phase is the presence of weak reflections off the lamellar axis. It would be difficult to observe off-axis reflections from the hydrated specimens described in the present article because of large mosaic spread of the multilayer. Consequently, we are reluctant to suggest that the secondary lattice of Fig. 5 arises from a lamellar phase. A more detailed examination of the off-axis diffraction is called for.

Acknowledgments

We gratefully acknowledge the advice and assistance of Dr. Meredithe Applebury. We thank Dr. J. Kent Blasie for his consultation, Dr. Wolfgang Baehr for help with the preparations, and Dr. Jim Milch for his support and encouragement. The data for Fig. 5 were acquired at the Stanford Synchrotron Radiation Laboratory. We thank SSRL and Dr. Blasie for aid in acquiring these data. This work was supported by the NIH under Grant EY-02679 and the DOE under grant EY 76-S-02-3120.

References

1 Gruner, S.M., Barry, D.T. and Reynolds, G.T. (1980) Fed. Proc. 39, 1807 (Abstr.)
2 Barry, D.T. (1979) Ph.D. Thesis, Princeton University, Princeton, NJ
3 Schwartz, S., Cain, J.E., Dratz, E. and Blasie, J.K. (1975) Biophys. J. 15, 1201–1233
4 Blasie, J.K., Dewey, M.M., Blaurock, A.E. and Worthington, C.R. (1965) J. Mol. Biol. 14, 143–152
5 Blasie, J.K., Worthington, C.R. and Dewey, M.M. (1969) J. Mol. Biol. 39, 407–416
6 Santillan, G. (1975) Ph.D. Thesis, University of Pennsylvania, Philadelphia, PA
7 Hamanaka, T. and Blasie, J.K. (1978) in Diffraction Studies of Biomembranes, Muscles and Synchrotron Radiation (Mitsu, T., ed.), University of Tsukuba, Ibaraki, Japan
8 Gruner, S.M. (1977) Ph.D. Thesis, Princeton University, Princeton, NJ
9 Liebman, P.A. and Pugh, E.N., Jr. (1979) Vision Res. 19, 375–380
10 Barry, D.T., Costello, M.J. and Gruner, S.M. (1980) Exp. Eye Res. 30, 501–510
11 Abrahamson, E.W. and Fager, R.S. (1973) Curr. Top. Bioenerg. 5, 125–200

12 Gruner, S.M. (1981) Rev. Sci. Instrum. 52, 134–136
13 Farnsworth, C.C. and Dratz, E.A. (1976) Biochim. Biophys. Acta 443, 556–570
14 Stone, W.L., Farnsworth, C.C. and Dratz, E.A. (1979) Exp. Eye Res. 28, 387–397
15 Reynolds, G.T. and Milch, J. (1976) Adv. Electron. Electron Phys. 40B, 923–943
16 Reynolds, G.T., Milch, J. and Gruner, S. (1977) IEEE Trans. Nucl. Sci. NS-24, 501–510
17 Gruner, S.M., Milch, J.R. and Reynolds, G.T. (1978) IEEE Trans. Nucl. Sci. NS-25, 562–565
18 Reynolds, G.T., Milch, J.R. and Gruner, S.M. (1978) Rev. Sci. Instrum. 49, 1241–1249
19 Hosemann, R. and Bagchi, S. (1962) Direct Analysis of Diffraction by Matter, North-Holland, Amsterdam
20 Worthington, C.R., King, G.I. and McIntosh, T.J. (1973) Biophys. J. 13, 480–494
21 Nelander, J.C. and Blaurock, A.E. (1978) J. Mol. Biol. 118, 497–532
22 Guinier, A. (1963) X-Ray Diffraction in Crystals, Imperfect Crystals and Amorphous Bodies, W.H. Freeman, San Francisco
23 Corless, J.M. (1972) Nature 237, 229–231
24 Blaurock, A.E. and Wilkins, M.H.F. (1972) Nature 236, 313–314
25 Chabre, M. (1975) Biochim. Biophys. Acta 328, 322–335
26 Levine, Y.K. (1973) X-Ray Diffraction Studies of Membranes, in Progress in Surface Science, Vol. 3, Part 4 (Davison, S.G., ed.), Pergamon Press, Oxford
27 Quinn, P.J. and Chapman, D. (1980) CRC Crit. Rev. Biochem. 8, 1–117
28 Clark, N.A., Rothschild, K.J., Luippold, D.A. and Simon, B.A. (1980) Biophys. J. 31, 65–96
29 Rothschild, K.J., Rosen, K.M. and Clark, N.A. (1980) Biophys. J. 31, 45–52
30 Gruner, S.M., Rothschild, K.J. and Clark, N.A. (1982) Biophys. J., in the press